JOINT EUROPEAN TORUS JET

JET–P(87)63

A.P.H. Goede, B.R. Nielsen
and E. Thompson

Physics Design of the Defelection Magnets of the JET Neutral Beam Injector

Physics Design of the Defelection Magnets of the JET Neutral Beam Injector

A.P.H. Goede[1], B.R. Nielsen[2] and E. Thompson[1]

JET-Joint Undertaking, Culham Science Centre, OX14 3DB, Abingdon, UK

[1]JET-Joint Undertaking, Culham Science Centre, OX14 3DB, Abingdon, UK
[2]Danfysik AIS, DK 4o4o Jyllinge, Denmark

Preprint of Paper to be submitted for publication in
Nuclear Instruments and Methods in Physics Research, Section A.

ABSTRACT.

This paper presents the ion optical calculations for the deflection magnets of the JET neutral injection system. The large amount of ion power to be handled (26MW) requires more accurate calculations than before. These include 3D magnetic field computations, raytracing and emittance calculations, the latter applied to a multiple aperture ion beam. The resulting power deposition profiles for the full energy ions (80keV hydrogen, 160keV deuterium) and for the fractional energy ions are reported.

1. INTRODUCTION

Additional heating at JET (Joint European Torus) is achieved, among other methods, by injection of powerful hydrogen or deuterium atom beams into the tokamak plasma from two beamline systems [1,2]. Each system can deliver a maximum of 10 MW deuterium beam power at 80 keV energy with a pulse duration of 10 seconds. At higher beam energy the system can deliver 160 keV D° beams (or, at equivalent energy per nucleon 80 keV H° beams) with about 7 MW of power to the tokamak plasma for 10 second pulse duration. Inside the neutral injection system the ion deflection magnets separate out the non-neutralised components of the extracted ion beams after neutralisation. The relatively low charge-exchange neutralisation efficiency at high beam energy (~ 25% for 80 keV per nucleon) requires a large fraction of the extracted ion beam power (~ 26 MW) to be deflected and dumped on actively cooled beam dumps inside the neutral injection box (NIB). The maximum power density that can be handled at the ion beam dumps (≈ 1 kW/cm^2) and the restricted space-envelope available for the dumps inside the NIB call for a careful magnet design. High emphasis was therefore placed during the design phase of the neutral injector to obtain accurate ion optical calculations for the deflection magnet.

The problem has been approached using three complementary methods

i) Analytic thin-lens approximation. The focussing properties in the plane orthogonal to the bending plane (the nonbend plane) due to the fringe fields at the entrance and the exit of the magnet can be represented by thin lenses of focal length f given by $f = \rho/\tan\alpha$, where ρ is the bending radius of the ions and α the angle of incidence with respect to the normal of the entrance

poleface. This simple linear analysis has proved to be useful especially during the conceptual design when several different types of configuration were assessed. It was also used later for analytic corrections on numerically obtained results.

ii) Accurate calculation of the ion trajectories requires knowledge of the exact shape of the fringe field and this has been obtained by numerical methods. The large ratio of gapwidth to bending radius of the JET magnets produces an extended fringe field, where the shape depends on parameters such as the coil position and the saturation level in the iron circuit. These modify the effective position and strength of the equivalent thin lenses used in the above analysis. The numerical computations, first in 2D later in 3D, were used to define the precise shape of the polefaces of the magnet. Power density profiles on the various ion dumps were derived by ray-tracing the beam contour through the magnet, and as a result, the geometry of the system of magnet and dumps was defined.

iii) The above analysis does not take into account the finite emittance of the beam. Although in the region of interest the beam optics are dominated by the geometric steering of the individual beamlets comprising the multiple aperture ion beam, the emittance effects are important in predicting the power density profile near the edge of the beam. In any case, at positions where the beam crosses over, emittance calculations are essential for calculating the beam power density.

Conservation of emittance is a well-known technique used in the study of beam transport in high-energy accelerators, but to our knowledge this is the first time [3] this technique has been applied in relation to the transport of multi-aperture (multi-ampère) ion beams through a magnet. One interesting feature arising from these studies is that the waist of the individual beamlets (upright beamlet ellipse in phase-space) does not coincide with the waist of the total beam (upright super-ellipse in phase-space) but is predicted to occur some distance beyond.

In this paper we shall present the conceptual design of the magnet in section 2 and the physics design, comprising the ion optical calculations in section 3. The resulting power density profiles calculated at the ion dumps for the full and fractional energy ion beam components are documented in section 4. The ion optical calculations for the so-called 'devious' particles, created by charge changing reactions that take place inside the magnet, have already been published [4], as have the details of the engineering design of the magnet [5]. Preliminary results on the operational experience gained with the the magnet operating with hydrogen and deuterium beams are reported in [6,7]. These include measurements of the total power and the power density distribution on the full and fractional ion dumps.

2. CONCEPTUAL DESIGN

The beamline configuration for the given injector specification revolved to a large extent around the choice of magnet to deflect the non-neutralised beam fractions out of the path of the transmitted fast neutrals. Various configurations were considered with the aim of

- minimising the overall length of the beam-line in order to give maximum beam transmission to the tokamak
- minimising the length of the magnet along the beam-line axis in order to reduce re-ionisation losses of the neutral beams as they pass through the magnet
- minimising the sensitivity of the ion optics with regard to unquantified effects such as space-charge expansion of the ion beam inside the magnet.

The chosen configuration is shown in Figure 1. Each JET injector contains eight ion sources which are coupled in four pairs by the deflection magnet, each magnet deflecting the beams of two ion sources. The full-energy ion beams are deflected in transmission through ~ 90°, whereas the half and third energy ions resulting from the breakup of extracted molecular ions (H_2^+, H_3^+) are turned through ~ 270°. This solution has the advantage that the magnet provides a baffle for differential pumping, and the gas backstreaming from the full-energy ion dumps has no direct sight of the torus port. It thus reduces the neutral beam losses due to reionising collisions with the background gas. Furthermore, it minimizes the overall length of the injector, which is important for maintaining a high neutral beam transmission and remaining inside the available torus hall floor area. With this configuration the dump power distribution is relatively insensitive to a shift or broadening of the ion beam focus, which may result from space charge forces.

3. PHYSICS DESIGN

3.1 Thin Lens Analysis

The ion optics of the magnet were first studied by linear matrix theory where the magnet is represented by thin lenses connected by a drift region. Acceptable power density levels at the ion dumps require a parallel or slightly divergent exit beam with magnification ≥ 1 at the dump both in the bend-plane and in the nonbend-plane. These requirements define a regime in parameter space for the entrance and exit poleface angles α and β and for the bending angle ϕ of the magnet. The transfer matrices in the bend plane B and the nonbend plane N are given by (e.g. H A Enge [8] Table I)

$$B = \begin{bmatrix} \dfrac{\cos(\phi-\alpha)}{\cos\alpha} & \rho \sin\phi \\ -\dfrac{\sin(\phi-\alpha-\beta)}{\rho \cos\alpha \cos\beta} & \dfrac{\cos(\phi-\beta)}{\cos\beta} \end{bmatrix}$$

$$N = \begin{bmatrix} 1 - \phi \tan\alpha & \rho\, \phi \\ \dfrac{-\tan\alpha - \tan\beta + \phi \tan\alpha \tan\beta}{\rho} & 1 - \phi \tan\beta \end{bmatrix}$$

In order to study the properties of these transfer matrices, first consider the conditions for a parallel input to parallel output beam (telescopic system) which require the bottom-left matrix elements to be zero. For the bend plane this leads to the condition $\phi = \alpha + \beta$ which is accomplished with a parallel sided magnet. For the nonbend plane it leads to the condition $\phi = \tan^{-1}\alpha + \tan^{-1}\beta$. A simultaneous solution satisfying both conditions exists only for bending angles $\phi \geq 98.6°$.

This large bending angle is not optimally suited to the NIB geometry. The condition can be relaxed however to lower bending angles when allowing for a slightly divergent output beam. In the bend plane this results in $\phi < \alpha + \beta$ which can be accomplished by a wedge shaped magnet, the wedge angle being the difference between the angles ϕ and $\alpha + \beta$.

Magnification ≥ 1 of a parallel output beam requires that the magnitude of the top-left matrix elements is ≥ 1. For the bend plane this leads to $\alpha \geq \phi/2$. Together with the condition for parallel transfer in the bend plane it also implies $\alpha \approx \beta$. The presence of a drift space between magnet exit and dump relaxes this condition on the entrance angle depending on the length of the driftspace.

This simple analysis of the ion optics of the magnet thus leads to the result that the magnet needed is approximately parallel sided with a bending angle of $90° < \phi < \alpha + \beta$, angled with respect to the beams at an angle $\alpha \approx \beta \geq 45°$ and with a wedge angle of a few degrees subtended between polefaces. In this situation the finite angle of incidence causes the ion beam to cross over in the nonbend plane at locations $\rho/\mathrm{tg}\alpha$ away from the entrance poleface. A good match between the emerging ion beam and the acceptance of the ion beam dump is achieved when the beam dump is arranged parallel to this beam cross-over line, i.e. with the beam dump approximately parallel to the entrance poleface of the magnet.

3.2 Numerical Calculations

The large gap width D to bending radius R (D/R ≈ 0.4) of the JET magnet produces an extended fringe field which modifies the position and strength of the thin lenses considered in the previous section. For example, in the far fringe field the incoming ion is bent towards the normal of the pole face reducing the effective angle of incidence before the planar field components, that produce the nonbend plane focussing, reach their full strength (cf [5] Figure 4). This causes a reduction of the nonbend plane focussing compared with the thin lens prediction. On the other hand, at higher magnet excitation, saturation in the iron return yoke creates a reversal in the fringe field which produces the opposite effect. Furthermore, the ion beam essentially entirely fills the magnet aperture (beam width to gap width ratio ≃ 0.65), whilst the linear equations only apply for particle trajectories near the central ray (paraxial ray approximation). Later in this section we shall discuss the existing methods for correcting the thin lens analysis with the aid of computed and measured magnetic field profiles. Prior to this, a more realistic representation of the fringe field can only be obtained by numeric means.

Two dimensional computations, taking into account the coil current and the finite non-linear permeability of the iron circuit, served as the basis of a parametric study in which the poleface and bending angles were varied. A three-dimensional study, required because the beam passes close to the end return yokes, was performed on this basis and in several iterations the system was optimised. The two-dimensional studies and the first three-dimensional study were carried out [9] employing the GFUN code [10]. Final optimisation was performed by JET using the TOSCA-3D code [11].

The following results emerged:

i) An angle of incidence $\alpha > 45°$ magnifies the full energy beam in the bend plane. A larger magnification is required for the outer beam because of its closer proximity to the full energy ion dump which is constrained by the height of the NIB. The inner beam (adjacent to the equatorial plane of the torus) allows a smaller angle of incidence because of the longer drift length available to the diverging exit beam. The total amount of power in the full energy component is ~ 3 MW per beam for an assumed [12] extracted species ratio $H^+ : H_2^+ : H_3^+ = 84 : 12 : 4$. This clearly defines the full energy ion component as the first priority for optimisation of the ion optics.

ii) A small angle of incidence reduces the nonbend plane focussing (and it also reduces the total length of the beam line). This is important for the fractional energy ions reflected through 270° (refer Figure 2), which become intercepted by the poleface liners and form a second cross over near the equatorial plane of the NIB generated by the exit poleface lens. Reduction of the power density at these surfaces favours an angle of incidence $\alpha < 45°$. This refers to the inner beam. The outer fractional energy ion beam is intercepted inside the magnet near the outer return yoke rather than at the equatorial plane, because space for 270° turnaround of the outer beam ions was restricted by the height of the NIB. This demands a larger angle of incidence for the outer beam in order to create a sufficient drift space between the cross-over and the dump at the outer return yoke. The total amount of power involved in the fractional energy ion beams is ~ 250 kW/beam.

iii) The optical properties of the negative ions, bouncing off the fringe field, heavily divergent and creating a ribbon focus at the entrance poleface liner, lead to conflicting requirements for the poleface angle. However, the small amount of power involved (~ 6.5 kW/beam) allocates lowest priority to this requirement.

The result of this optimisation process is shown in Figure 2. The angle of incidence for the inner beam was chosen to be 40° and for the outer beam 46°. A wedge angle of 7° is subtended between entry and exit pole face edges. The requirements for the optics of the outer and inner beams are combined through a 5 cm step at the entrance poleface, influencing to some extent the turned round fractional energy ions. By judicious choice a step in the exit poleface could be avoided. This simplified the design and more importantly the actual manufacture of the magnet. In between the poleface edge and the coil a 3 cm space was left open to allow for retroactive fitting of iron poleface shims to fine-tune the magnet optics after manufacture and test. Also shown in Figure 2 are sample ion trajectories for the full, fractional and negative ion components together with the calculated power densities (kW/cm^2) on the full energy dumps. The positions of the beam crossovers are marked by open circles. The beam cross-overs can be seen in detail in Figure 3, where the particle trajectories in the nonbend plane are shown.

The power density on the dumps was derived by tracking selected particles through the magnet, with initial conditions characterised by the entrance beam envelope. Beam envelope data were generated numerically by the ZAP-code [1], which models the beam as an array of Gaussian emitters of specified divergence, focus and steering. The

peak power density on the dumps derives from tracing the 50% density contour of the power density profile, assuming that all the beam power is contained within that contour (top-hat distribution). This is a reasonable approximation in our case where the beam profile is dominated by geometric steering rather than beamlet divergence (drift length less than 3.5 m). The procedure has the advantage that only a limited number of trajectories need to be traced per beam, but requires justification from emittance calculation.

3.3 Emittance Calculations

Single particle tracing codes cannot directly predict the beam envelope unless a large number of particles are traced. However, as will be shown in this section, the individual trajectories can be used to determine the focal properties of the magnet, which subsequently can be used to trace the emittance envelope through phase space. The power distribution in planes normal to the beam may then be calculated and deconvoluted on the beam intercepting surfaces.

The JET beam is composed of an approximately rectangular array of 262 beamlets of given divergence and steering extracted from an ion source of approximately 18 x 45 cm^2 extraction area. The first step in constructing the 'super-beam' emittance is to define the object for the beam optics. This task is complicated by the fact that space charge, gas scattering and molecular ion break-up in the extraction and neutraliser region are difficult to quantify. To overcome this problem we made use of experimental emittance observations on a reduced size JET extraction geometry [13], later confirmed for the full size

geometry [14]. The experimental result yields a Gaussian beamlet distribution of normalized emittance $\varepsilon_n = 0.17\ \pi$ mm mrad (e^{-1} contour) and a position of the 'virtual' object located near the extraction plane.

Figures 4 and 5 show the constructed emittance diagrams in the bend plane (x) and non-bend plane (y). The width of the individual beamlets follows from the measured emittance assuming a ± 0.5° beamlet divergence, the spacing follows from the extraction aperture row spacing. The tilt in the super-beam envelope is determined by the steering of the individual beamlets toward a common focus (f_x = 14 m, f_y = 10 m). Note that the drifted emittance diagram at the magnet entrance shows overlapping beamlet ellipses which means that the individual beamlets have merged. The implication is that in real space the beam profile can be constructed to good approximation from the super-envelope of the emittance diagram. This is illustrated in the bottom half of Figures 4 and 5 where the beam profile derived from the super-envelope (dotted curve) and the summation of individual beamlet intensity distributions (drawn curve) are compared. The particle density in the super-envelope is assumed to be constant along its major axis (lines of constant beamlet particle density) and Gaussian along its minor axis (major axis beamlet ellipse). In a separate study this profile was also shown to be in good agreement with the prediction from the ZAP code as expected.

Having established the fact that the beam profile can be represented by the phase-space super-envelope we proceed to trace this envelope through the magnet to the dumps. The results are shown in Figure 6

(bend plane) and Figure 7 (non-bend plane) for the inner beam, together with the calculated beam profiles. The crosses on the envelopes indicate the 50% beam contours for which the focussing properties of the magnet were established numerically as discussed in the previous section. The corners of the diagram represent the e^{-1} beamlet contours which can be shown to correspond to the 8% and 92% super-beam contours. These are also traced numerically.

One observes in the bend plane (Figure 6) at the magnet exit a slight compression of the beam (position 4) before expansion takes place at the dump (position 5). In the non-bend plane (Figure 7), the beam crosses over inside the magnet (position 3), whilst the cross-over of the individual beamlets (upright beamlet ellipses) occurs at some distance downstream (near position 4). This is an interesting feature of the magnet optics and would allow direct experimental observation. It would show up as a layered structure in the beam ($\approx$ 1 mm layer width) across the exit gap of the magnet along a line of sight approximately parallel to the magnet exit pole face. The power densities calculated in the beam and beamlet cross-overs of the inner beam are 60 and 40 kW/cm^2 respectively. The transport of the outer beam qualitatively evolves in the same way with slightly higher power densities in the cross-overs.

It is noted that at the dump the power density profile has retained its approximately trapeziodal shape. This result is surprising in the sense that the neutral beam at this distance from the source (~ 5 m) becomes divergence dominated. The explanation relates to the large angular deflections imparted by the magnet on the beam relative to the beamlet divergence. An important implication is that our approach of

the previous section to derive the peak power density from tracing the 50% beam contours, is justified.

A typical power density profile on the full energy ion beam dump derived from emittance calculations and compared with 50% contour tracing is shown in Figure 8. Agreement between the two is good in the beam centre, with the expected profile smoothing in the emittance calculation to appear at the beam edge. The peak power density occurs approximately halfway down the beam dump elements, not at the apex. This is a result of the V-shaped geometry of the dumps [15] where, away from the apex, the increased angle of incidence and the reduced beam width combine to produce higher power densities.

3.4 Analytic thin lens corrections

Analytic corrections to the thin lens formulae take into account the extended fringe field and are important in our case in order:

- to carry out a sensitivity analysis on the magnet poleface angle using a computed 2D fringe field profile
- to correct the numerical calculations with measured magnetic field profiles after manufacture of the magnet.

The analytic corrections aim to define an effective poleface angle and require knowledge of the nonbend plane fringe field integral $I_2 = -\int_{-s_1}^{\infty} dh \int_{s}^{\infty} h \, ds$, where s_1 is the normalised distance to the virtual field boundary, s the normalised distance in units of the gap width D and h(s) the normalised fringe field profile as defined by H A Enge in units of the constant field inside the magnet gap (see [8] Ch 4.2.3).

Measured values of the JET magnet yield I_2 = 0.22 (inner magnet) and I_2 = 0.16 (outer magnet). These results are derived from Figure 4 in [5]. These values are in disagreement with the values quoted in literature [8], which range from I_2 = 0.414 to I_2 = 0.708. The difference can be explained by the fact that the fringe field of the JET magnet has a much sharper field fall-off than the field profiles quoted in literature, because of its relatively small sized coil positioned close to the iron (compare Figure 4 in [5] with Figure 17 in [8]).

The above result is useful for correction of the numerical ion optics calculations on the basis of measured fringe field profiles. As reported in [5], the measured profiles were found to be less steep than the numeric profiles. The effect of this discrepancy on the ion optics has been assessed in the following way:
The measured field profile h(s) yields an effective angle of incidence α_m through the measured fringe field integral I_2, whilst the computed profile similarly yields an effective α_c. The ratio tan α_m/tan α_c then yields the correction by which the computed focal length needs to be changed. The above correction yields a 4% weaker focussing in hydrogen and a 5% weaker focussing in deuterium operation respectively. The calculated power densities turn out not to be very sensitive to this change with the exception of the outer fractional energy ion dump where the proximity of the cross-over to the dump surface creates an ~ 15% increase in the power density.

4. RESULTS

4.1 Full energy ion dump power distribution

The full energy ion dump consists of twenty beam stopping elements mounted as pairs in V-form with a 25° subtended angle to reduce the surface power density [15]. The dimension of each element is approximately 11 cm wide, 60 cm long and 3 cm thick. They are vertically stacked in the geometry indicated in Figures 1 and 2. The power distribution calculated in the long direction of each element (nonbend plane) is shown in Figure 9. The distance Δy is measured from the apex. The power density distribution in the bendplane is shown in Figure 10, calculated at a fixed distance from the apex for each element (Δy = constant).

The following assumptions were made in this calculation:

- 80 keV hydrogen ion beams of 3080 kW each (species ratio 84:12:4)
- ± 0.5° beamlet divergence
- perfect alignment and steering
- no poloidal stray field deflection
- no space charge effects
- no charge exchange beam losses inside the magnet.

According to these calculations the peak power loading of the elements always stays below 1.2 kW/cm^2 whilst the total power per element does not exceed 400 kW. These figures are within the

design limits of the dump elements [15]. At the apex of the dump where EB-welds define a lower mechanical stress limit, the power densities remain within the specified 1 kW/cm^2 limit. An important aspect of the calculations is that also the sides of the elements receive a finite power loading depending on the angle of incidence of the beam in the bend plane. Calculated power densities range from 0.2 to 0.5 kW/cm^2 depending on the range of variation in the magnetic field value. In deuterium operation detailed differences in the power distribution exist. The peak power density however stays within the specified limits. The differences are caused by the different fringe field distribution, as a result of the onset of saturation in the iron circuit.

4.2 Fractional energy dumps and liners

The outer fractional energy ion beams are intercepted near the outer return yoke of the magnet whilst the inner beams are collected near the equatorial plane (see Figures 1 and 2). Localised high power densities are calculated along the centre lines of these dumps. For the outer beam this is caused by the proximity of the ribbon focus in combination with the nonbend plane beam compression. For the inner beam the magnet exit lens creates a second beam cross-over at the equatorial plane. In order to overcome this problem the beam stopping elements are made of two banana-shaped sections, with the cleavage between adjoining elements at the centre line of the structure, thus reducing the power density at the inclined surface. The

calculations are a sensitive function of the species ratio assumed. For an unfavourable 70:20:10 species ratio and a 1 cm beam to dump misalignment the design stays within the 1.2 kW/cm^2 peak power density design limit of the dump.

The power density distribution of the various species at the magnet liners is shown in Figure 11. Peak power densities are < 50 W/cm^2 at the ribbon point of the half energy ions and < 100 W/cm^2 for the total beam at the inclined surface of the entrance scrapers (both assuming ± 1 cm misalignment and an unfavourable species ratio). The total power intercepted by one liner side is 75.5 kW (125 kW including misalignment and unfavourable species). These figures allow for a liner design based on simple edge cooled copper plates, cooled during the off-duty period. Peak power densities and total powers are listed in the caption of Figure 11.

5. CONCLUSION

The deflection magnet-ion dump system of the JET neutral injector, required to safely handle 26 MW ion power pulses of 10 sec duration, forms perhaps the most critical component of the JET beam line. In this paper the ion optics problem has been approached by linear matrix theory, ray tracing through computed 3D magnetic fields and emittance calculations. The bulk of the power density calculations has been obtained by ray tracing a limited number of particles and is justified by emittance calculations. By this method the peak power density on the full

energy ion dump, and the power distributions on the fractional energy ion dumps and magnet liners have been obtained. Also the power distribution of the 'devious' particles (charge changing products created inside the magnet) were determined by this method. In critical areas (e.g. the full energy ion dump) the detailed power profile must be derived from emittance calculations in order to take account of the beam profile. Emittance calculations are also essential for the calculation of the power density in the beam cross-over. Prior to numeric calculations linear matrix analysis was useful to define the overall geometry of the magnet-ion dump system. Analytic methods were also useful after manufacture of the magnet for correction of the ion optics calculations with measured magnetic field profiles.

Acknowledgement Drs J H Coupland, A Baynham and T Randle of Rutherford Laboratory performed the initial 3D-GFUN calculations whilst Dr J Simkin provided help and advice with the 3D-Tosca calculations. Dr R S Hemsworth of JET provided the input beam envelope data and the neutral beam power profiles on the liners by employing the ZAP-code.

References

[1] G Duesing, H Altmann, H Falter, A Goede, R Haange, R S Hemsworth, P Kupschus, D Stork, E Thompson, Fusion Technology 11, 163 (1987).

[2] A P H Goede, C Challis, T T C Jones, A Stäbler, D Stork, E Thompson, Proc 14th Symp on Fusion Technology, Avignon (1986), Pergamon Press (1986) Vol 2, p 1139.

[3] A P H Goede, A A Ingersoll, P Kupschus, B R Nielsen, E Thompson, R S Hemsworth, Proc 12th Symp Fusion Technology, Jülich, FRG, Sept 1982, p.1321, published for the Comm of European Comm by Pergamon Press (1983).

[4] B R Nielsen, A P H Goede, R S Hemsworth, E Thompson, Vacuum 34 (1984) 37.

[5] A P H Goede, B R Nielsen, F Shone, T Sønderskov, E Thompson, to be published.

[6] H D Falter, R S Hemsworth, G H Deschamps, A P H Goede, T T C Jones, P Massmann, H J Mead, Proc 11th Symp Fusion Eng, Austin Texas (1985) IEEE Cat N° 2251-7 Vol II pp 786-790.

[7] R S Hemsworth, G H Deschamps, H D Falter, P Massmann, Proc 12th Symp Fusion Eng, Monterey Ca (1987) IEEE Cat N° (paper 10-01).

[8] H A Enge, Deflection Magnets, Ch. 4.2 in Focussing of Charged Particles, Vol.II. Edited by A Septier, Academ. Press Inc., New York (1967).

[9] D E Baynham, J H Coupland, T C Randle, Rutherford Lab report RL-81-060 (1981).

[10] M J Newman, C W Trowbridge, L R Turner, Proc 4th Int Conf Magnet Technology, Brookhaven (1972).

[11] J E Simkin, C W Trowbridge, IEEE Proc 127, 368 (1980).

[12] A P H Goede and T S Green, Proc 8th Symp on Eng Problems of Fusion Research, San Fransisco (1979). IEEE Pub N° 79CH1441-5NPS New York (1979) 2, 680. and T S Green, Culham Neutral Beam Development Group, Proc 13th Symp on Fusion Technology, Varese (1984). Published for the Comm of Eur Comm by Pergamon Press (1984).

[13] G A Cottrell, A J T Holmes, Proc. 2nd Int. Conf. Low Energy Ion Beams, Bath, UK (1980), 13. Culham Neutral Beam Development Group.

[14] The Culham Neutral Injection Group, T S Green, et al, Proc 4th Int Symp Heating in Toroidal Plasmas, Varenna. Vol II (1984) 1073. Ed by H Knoepfel, E Sindoni. Monotypia Franchi, Città Castella (Perguia) Italy.

[15] R Haange, Proc 9th Symp on Eng Problems of Fusion Research, Chicago (1981). IEEE pub N° 81CH1715-2NPS New York (1981) 2, 1352.

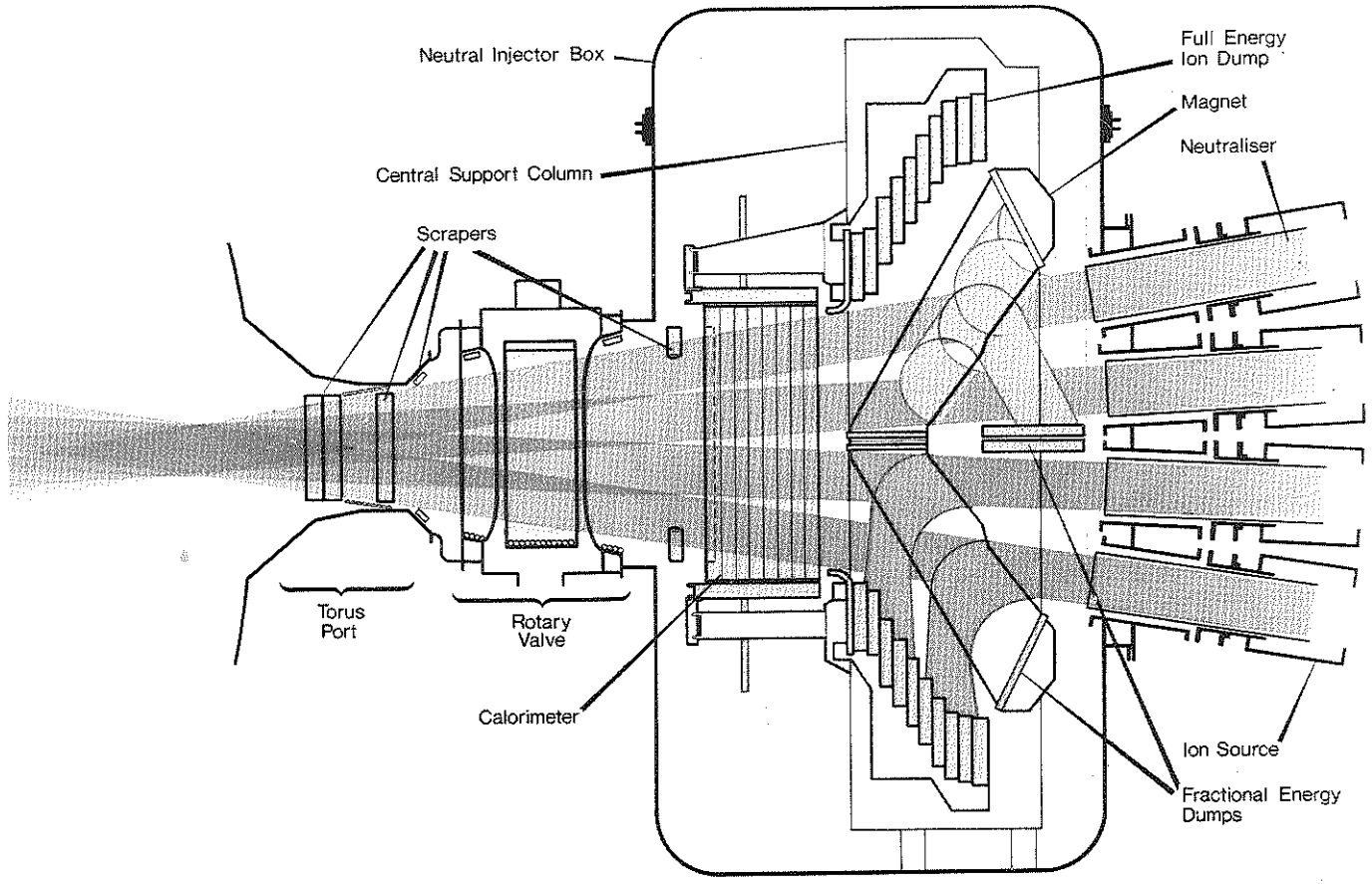

Fig. 1 Elevation of the JET neutral injector.

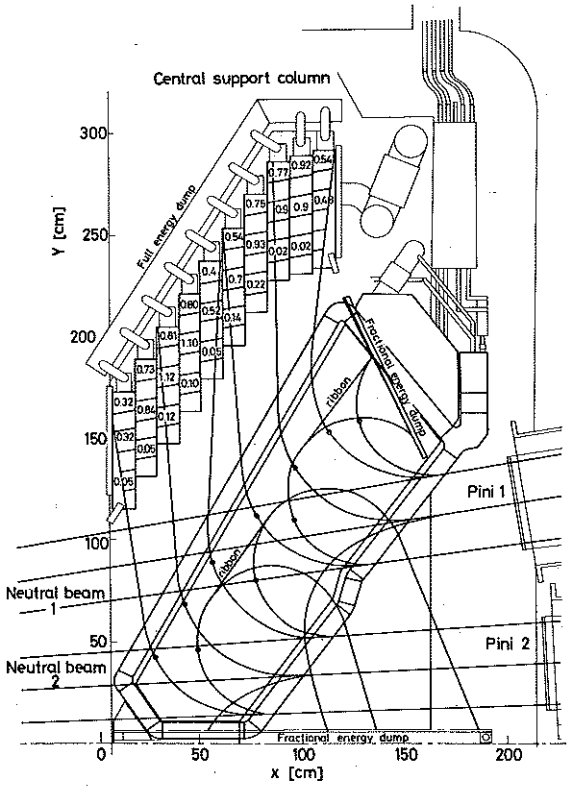

Fig. 2 Schematic of the JET bending magnets (one quadrant). Each magnet deflects the beams of two ion sources. Full energy particles are bent through 90°. Fractional energy particles are reflected through 270°. Power densities on the full energy ion dump are indicated. in kW/cm^2.

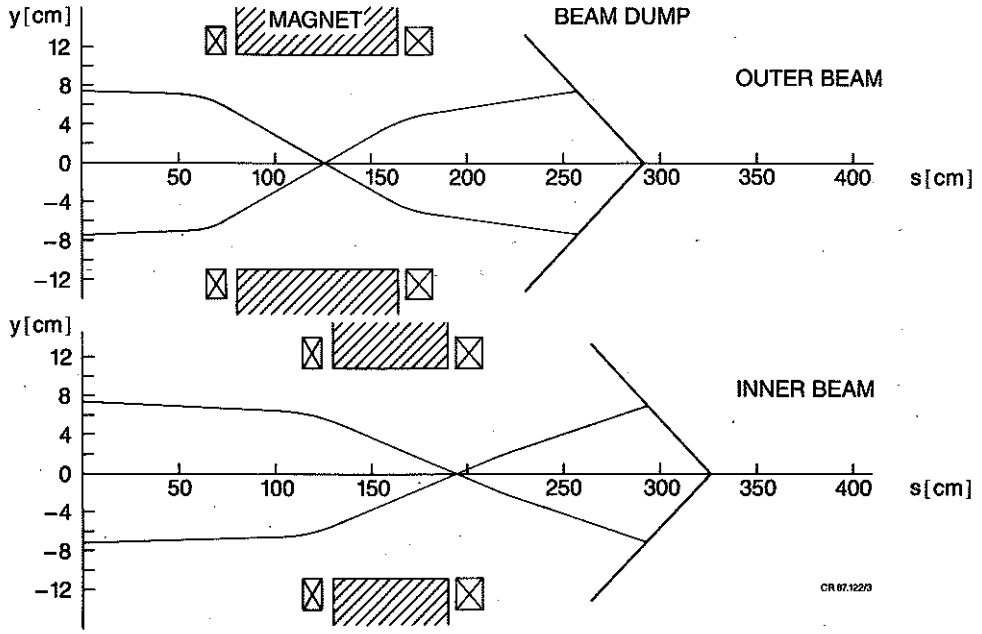

Fig. 3 Full energy ion trajectories in the nonbend plane mapped along the central ray.

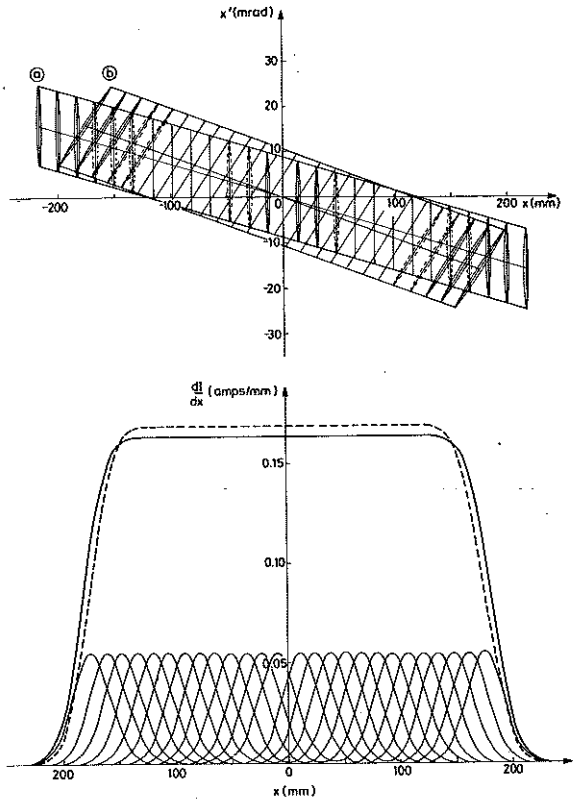

Fig. 4 Emittance diagram and beam profile in the bend plane (inner beam). Envelope represents the virtual object, envelope is the drifted diagram at the magnet entrance. Note that beamlet emittances overlap, i.e. beamlets have merged in real space. Calculated beam profiles at the magnet entrance from individual beamlet emittance (solid line) and super beam emittance envelope (dashed line) show good agreement.

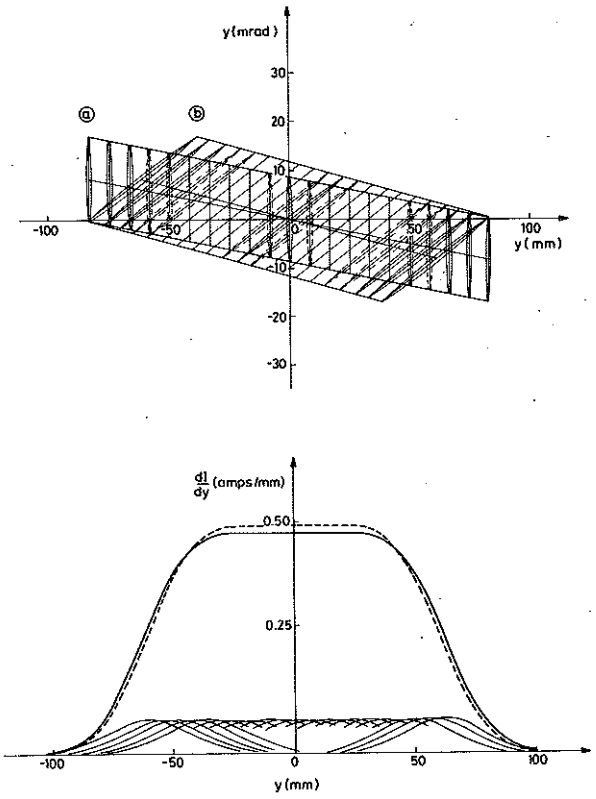

Fig. 5 Phase space diagrams similar to Figure 4, but in the nonbend plane. Magnet acceptance is indicated.

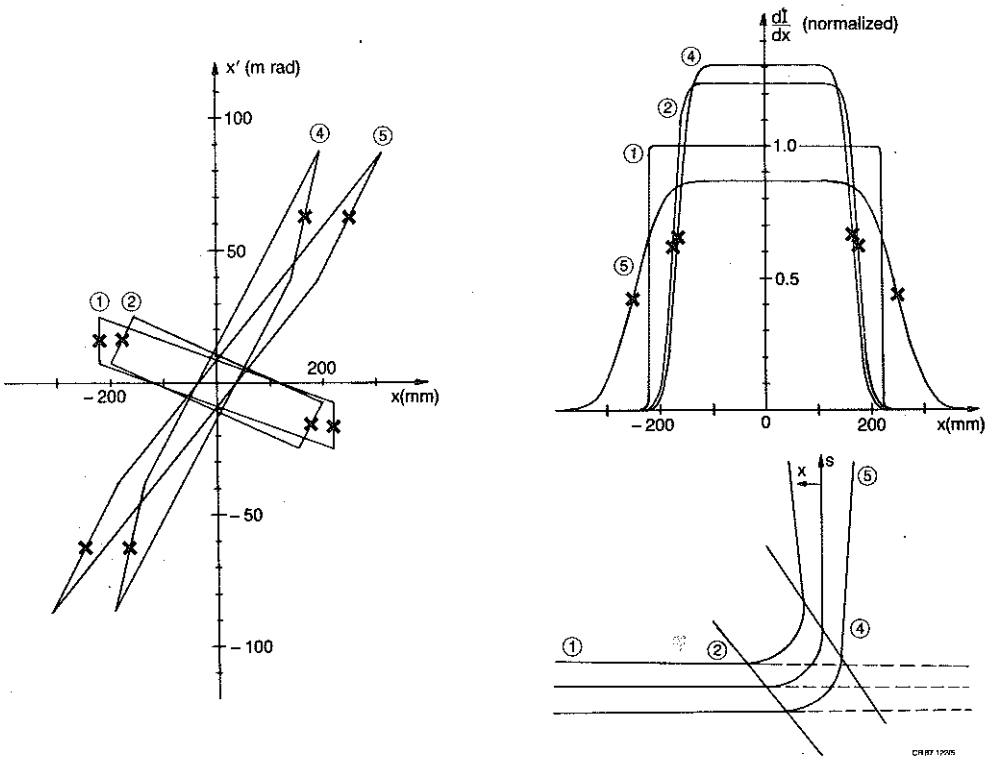

Fig. 6 Beam transport through the magnet in the bend plane. Crosses indicate the numerically calculated 50% contour trajectories. The emittance envelope is defined by the e^{-1} beamlet divergence corresponding to the 92% and 8% contour points on the super envelope.

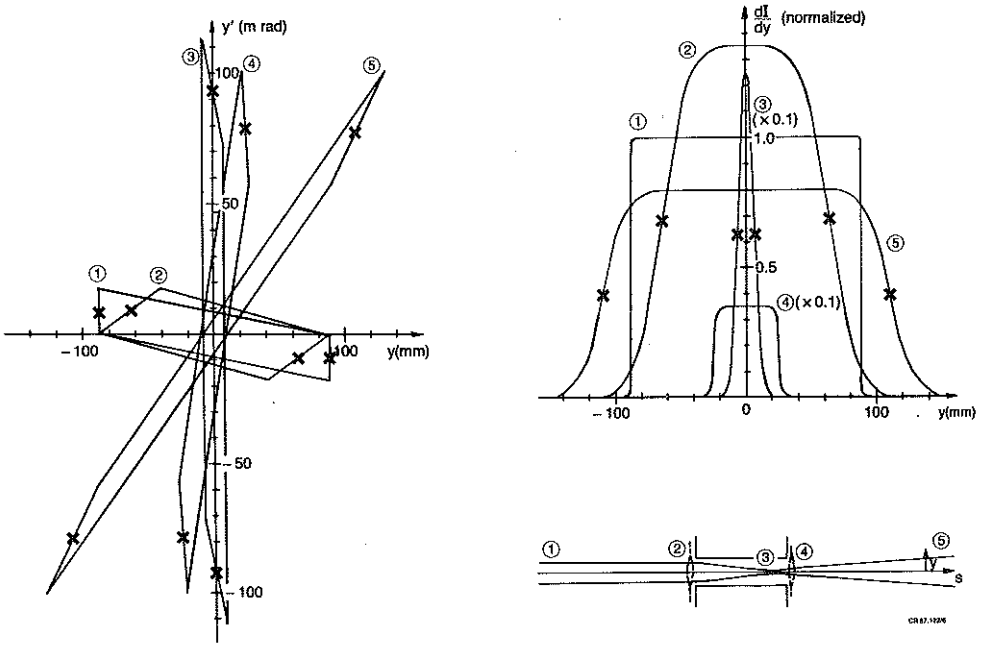

Fig. 7 Same as Figure 6 for the nonbend plane. Note the beam cross-over.

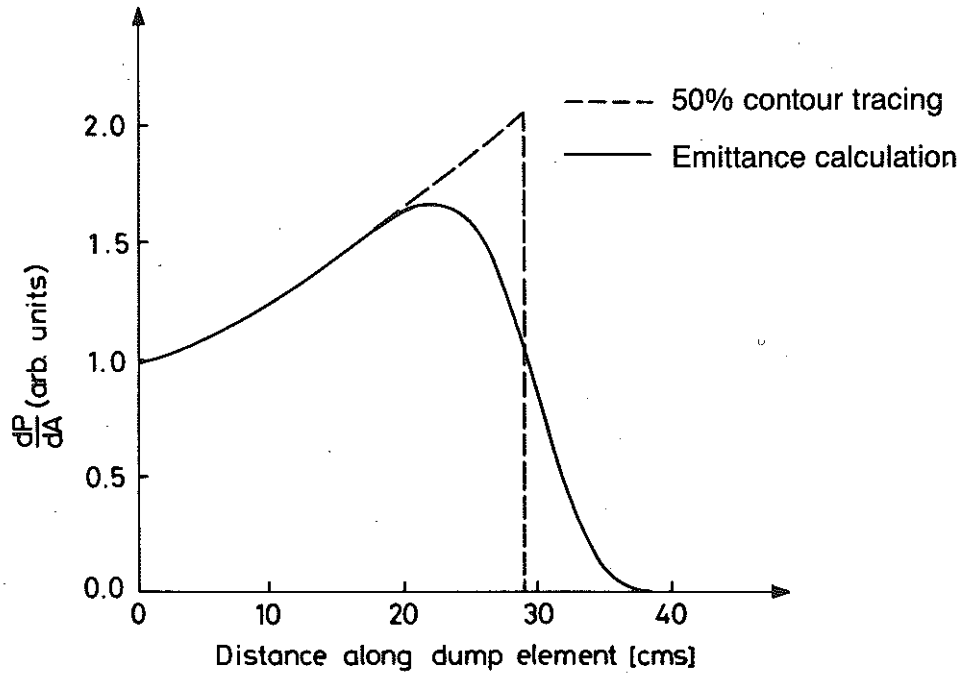

Fig. 8 Typical power density profile calculated along the full energy ion dump. The dashed curve represents a tophat beam distribution which shows good agreement with the emittance calculation (solid curve) at the beam centre, with the expected smoothing of the profile to occur at the beam edge.

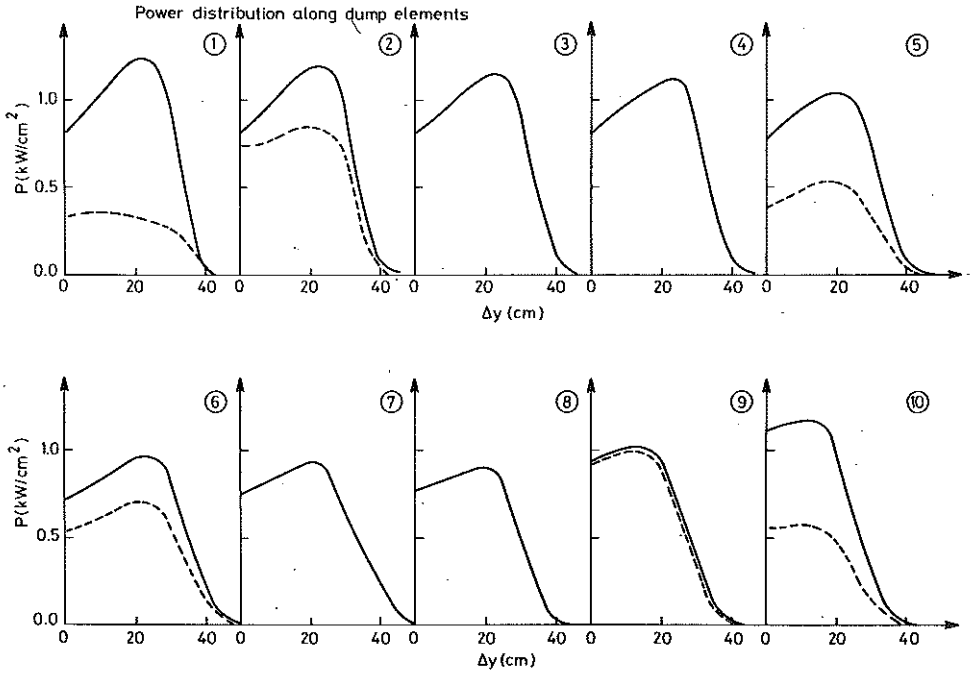

Fig. 9 Results of power deposition calculations for the full energy ion dump in the nonbend plane. Distance Δy is measured from the apex for each of the ten V-shaped elements comprising the dump. Dashed curves take into account the beam edge smoothing in the bend plane. Hydrogen at 80 keV.

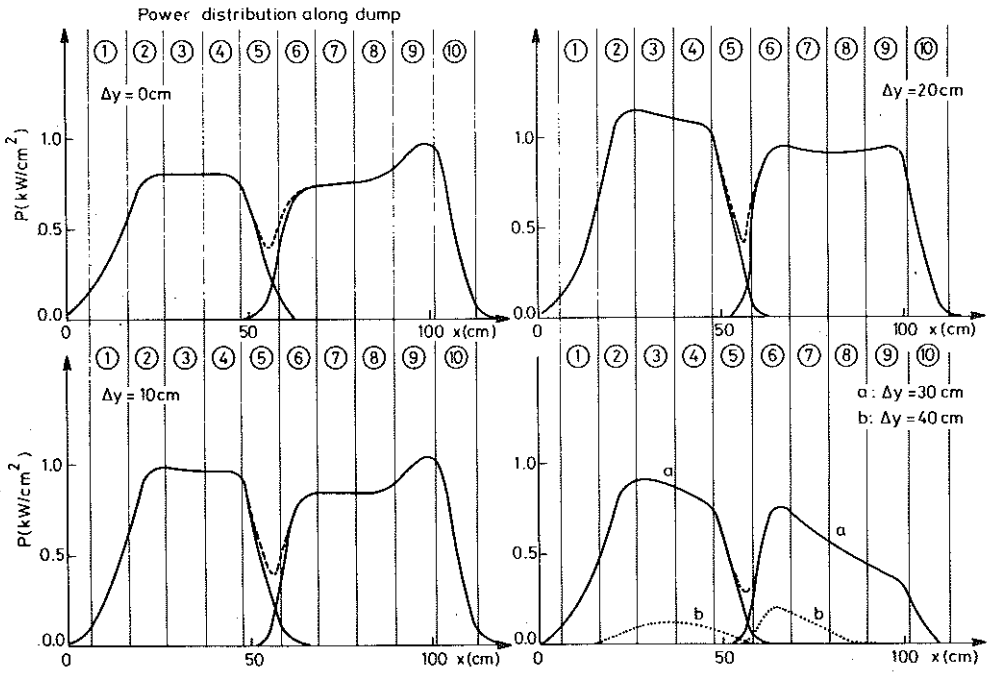

Fig. 10 Results of power deposition calculations for the full energy ions in the bend plane, across each of the ten beam dump elements. Distance Δy to the apex of the V-shaped elements is parameter. Hydrogen at 80 keV.

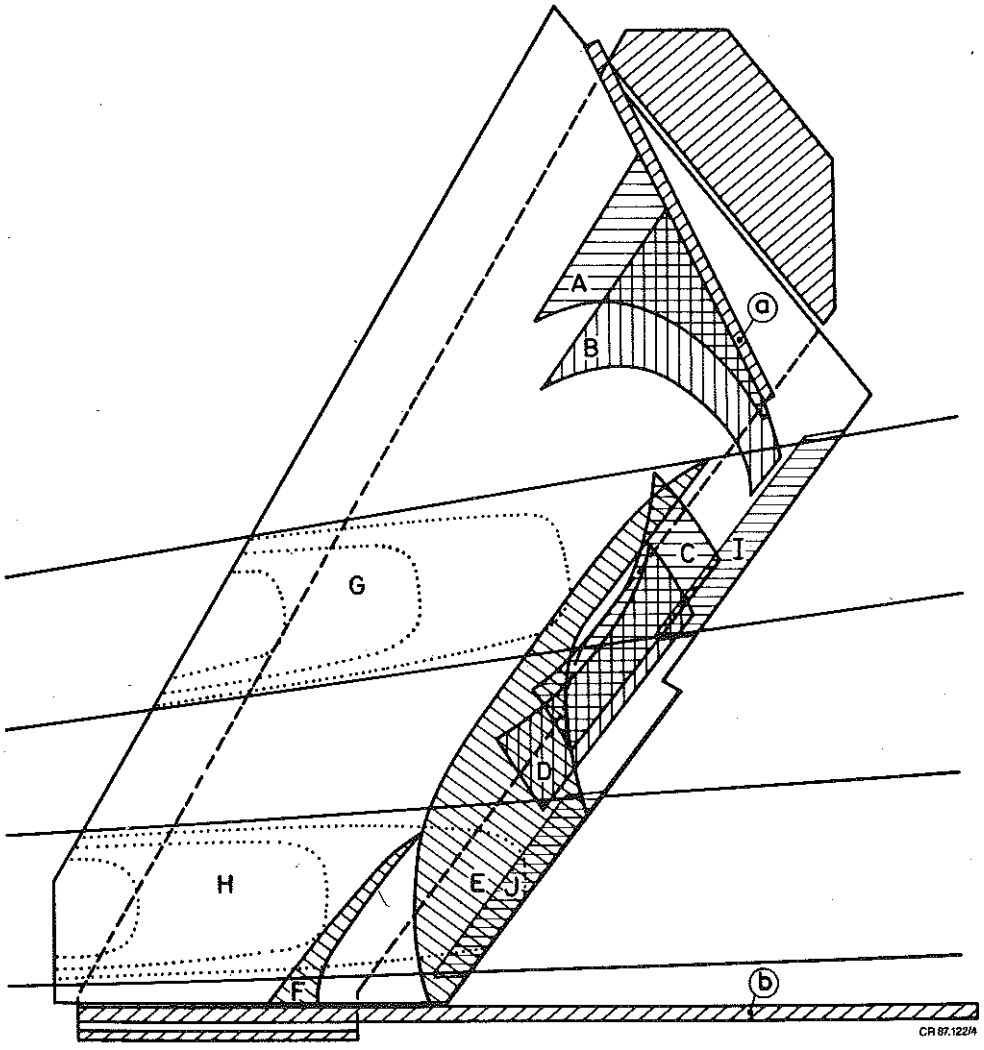

Fig. 11 Power density distribution on the magnet liners and fractional energy ion dumps. The various power deposition regions (peak power density in brackets) correspond to:

A,C	half energy ions (20 W/cm^2)
B,D	third energy ions (4 W/cm^2)
E,F	negative ions (9 W/cm^2)
G,H	neutral beam atoms (8 W/cm^2)
I,J	magnet entrance beam scraper (80 W/cm^2)
a,b	fractional energy ion dumps (0.9 kW/cm^2)

The total power on one liner side is 75 kW, on dump it is 207 kW and on dump it is 255 kW. These numbers refer to ideal conditions of no mis-alignment, no misfocus, beam divergence 0.5°, and species ratio 84:12:4. Nonoptimized conditions would increase the numbers.